Testing the Honeywell Durafet® for seawater pH applications

Todd R. Martz[1]*, James G. Connery[2], and Kenneth S. Johnson[3]
[1]Scripps Institution of Oceanography, University of California San Diego, La Jolla, CA, 92093
[2]215 E. Welsh Road, Maple Glen, PA, 19002
[3]Monterey Bay Aquarium Research Institute, Moss Landing, CA, 95039

Abstract

We report on the first seawater tests at 1 atm of the Honeywell Durafet® pH sensor, a commercially available ion sensitive field effect transistor (ISFET). Performance of this sensor was evaluated in a number of different situations including a temperature-controlled calibration vessel, the MBARI test tank, shipboard underway mapping, and a surface mooring. Many of these tests included a secondary reference electrode in addition to the internal reference supplied with the stock Durafet sensor. We present a theoretical overview of sensor response using both types of reference electrode. The Durafet sensor operates with a short term precision of ± 0.0005 pH over periods of several hours and exhibits stability of better than 0.005 pH over periods of weeks to months. Our tests indicate that the Durafet pH sensor operates at a level of performance satisfactory for many types of biogeochemical studies at low pressure.

The pH is of fundamental importance to contemporary studies of seawater chemistry. As a master variable of the CO_2 system, pH determines its speciation into carbonic acid ($H_2CO_3^*$), bicarbonate ion (HCO_3^-), and carbonate ion (CO_3^{2-}). Because the ocean has absorbed nearly one half of all anthropogenic CO_2 emissions (Sabine et al. 2004), surface seawater pH is decreasing at ~0.002 units yr^{-1}, while calcite and aragonite saturation horizons shoal at rates up to ~1 m yr^{-1} (Feely et al. 2004). The international scientific community predicts that this process will trigger significant ecosystem effects that may cascade into major socioeconomic problems (Raven et al. 2005; Schubert 2006). Ocean acidification has therefore been identified as a vital research issue (Fabry et al. 2008; Kleypas et al. 2006). Yet pH continues to be chronically undersampled in both space and time. This problem results from the combination of remoteness of the ocean and the fact that most pH measurements are carried out in ship-based laboratories.

*Corresponding author: E-mail: trmartz@ucsd.edu

While there have been numerous controlled experiments demonstrating the effects of ocean acidification on biological processes, there are few direct observations of the process itself because changes of –0.002 pH yr^{-1} require high quality measurements that are generally only practical with ship-based sample collection. The use of potentiometry to measure seawater pH has largely been abandoned by scientists interested in the oceanic CO_2 system because irreproducible differences and sensor drift between identical glass electrodes lead to nearly insurmountable difficulties in electrode calibration. The spectrophotometric pH measurement technique, refined by Robert Byrne and coworkers (1993) at the University of South Florida is now the basis of nearly all pH measurements made for studying the seawater CO_2 system. Discrete (Friis et al. 2004), underway (Bellerby et al. 2002), and profiling (Nakano et al. 2006) spectrophotometric pH instruments are increasingly common. Autonomous spectrophotometric pH analyzers (Liu et al. 2006; Martz et al. 2003; Seidel et al. 2008) that can operate in situ for months without calibration are now beginning to be used. Although spectrophotometry offers clear advantages over the glass electrode (Dickson 1993a), obtaining high quality measurements of seawater pH using indicator dyes in situ comes with certain limitations. Indicator dye must be introduced into a seawater sample before a measurement and a spectrophotometric blank must be frequently re-recorded to account for any changes in optical throughput. Thus, even the simplest spectrophotometric device requires a pump(s) and valve(s) to move and mix the seawater sample and indicator dye. Consequently, obvious limitations of autonomous spectrophotometric pH include slow response

time and high complexity. While it may be possible to achieve a response time of a few seconds using an underway system, power limitations of autonomous instruments severely limit flushing time between blank and sample, resulting in a response time on the order of minutes.

Clearly, there is a need for a pH sensor with improved simplicity and performance. The literature is filled with descriptions of novel solid-state pH sensors based on, to name a few, immobilized chromophores (Sedjil et al. 1998), immobilized fluorophores (Zhu et al. 2005), iridium oxide (Wang and Yao 2003), and yttria-stabilized zirconia (Ding et al. 2005). Yet none of these new technologies have proven capable of the high precision and accuracy demanded for seawater CO_2 studies.

Over the last 10 yr, a small number of research groups have begun measuring seawater pH using Ion Sensitive Field Effect Transistor (ISFET) technology (Le Bris and Birot 1997; Shitashima et al. 2002). The ISFET operating principle is explained by Bergveld (2003). Briefly, an ISFET is a Metal Oxide Semiconductor Field Effect Transistor (MOSFET) without a metal gate electrode over the conduction channel (Fig. 1). The conduction channel is covered by a thin insulating layer of amphoteric material such as silicon nitride (Si_3N_4), aluminum oxide (Al_2O_3), yttrium oxide (Y_2O_3), or tantalum pentoxide (Ta_2O_5). The pH of the solution at the insulator/solution interface controls the site-binding protonation/deprotonation state of the insulator material and, hence, the surface charge at the interface. The interfacial charge determines the strength of the electric field in the conduction channel of the FET, located between the source and drain. ISFETs are commonly operated by applying a constant drain-source voltage and using a feedback circuit to hold the drain-source current constant. A conventional reference electrode is used in lieu of the now removed gate. The analytical pH signal is proportional to the reference electrode to source voltage.

ISFET pH sensors offer a number of advantages, relative to glass electrodes. In particular, sensor impedance is much lower than in a glass electrode, which greatly reduces drift and noise due to stray currents. The work of Le Bris and Birot indicates that ISFET response may be insensitive to pressure, but their work did not focus on long-term stability. Shitashima and coworkers (2002) have also made important progress in seawater pH ISFET applications. Further, they addressed the problem of a suitable reference electrode, which has significant impacts on measurement accuracy. As suggested by Culberson (1981), an ion selective electrode half cell, reversible to a major seawater ion is a viable alternative to a conventional, liquid, or gel-filled reference electrode with a liquid junction that completes the circuit. Shitashima et al. (2002) have shown that a solid-state chloride ion selective electrode (Cl-ISE), exposed to the seawater sample, suffers little pressure hysteresis, unlike a liquid-filled Ag/AgCl reference electrode with a liquid junction.

The previous work with ISFETs in seawater has not addressed long-term drift, possibly because these studies were carried out with metal oxide insulator materials not ideally suited for sea-
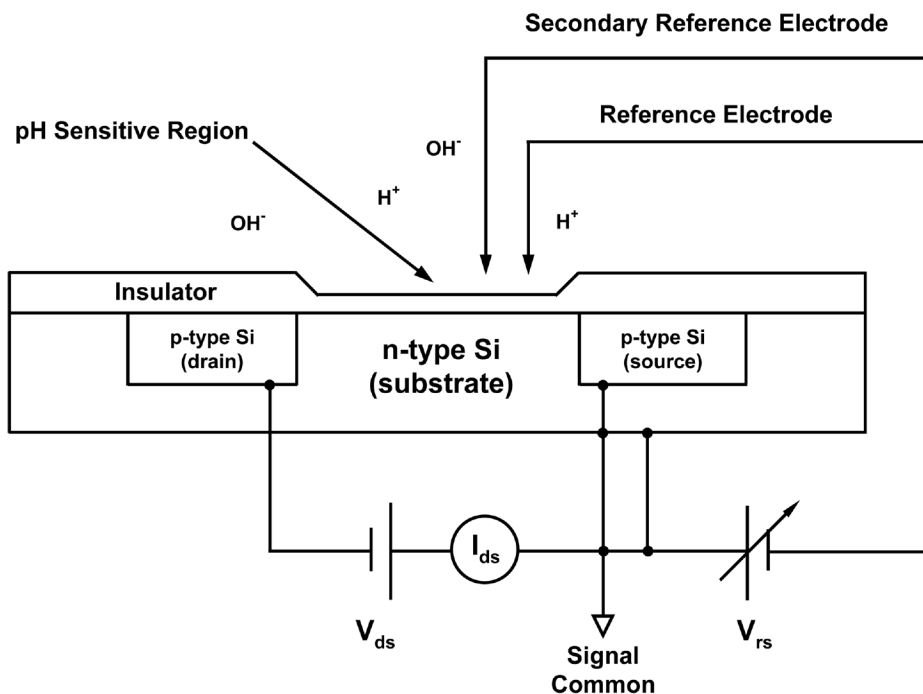

Fig. 1. Functional implementation of the ISFET operating principle. The Durafet is a p-channel enhancement mode ISFET, operated at a constant drain-source voltage and current. These conditions are obtained by adjusting an external reference electrode to source voltage (Vrs) to maintain constant Ids. The reference-source voltage (Vrs) obeys a Nernstian response to protons in solution. The secondary reference EMF is also measured versus signal common.

water media (Bergveld 2003), chip packaging that used resin coatings with limited lifetimes (Oelßner et al. 2005), or simply that these studies focused mostly on short-term applications such as single profiles and detection of waters influenced by hydrothermal vents. Here, we explore the use of a Honeywell Durafet ISFET sensor for seawater pH measurements over sustained periods in situ. Chip encapsulation technology has continuously improved over the last decade. However, questions remain regarding the lifetime of ISFET chip packaging and sensor stability over long periods in the ocean.

The Durafet is a combination electrode with an internal reference formed by a Ag wire in a AgCl and KCl saturated gel in contact with the test solution through a liquid junction. As shown by our preliminary results below and by others (Sandifer and Voycheck 1999), Honeywell's commercially available ISFET pH sensor, using the internal reference, appears to exhibit remarkable stability at 1 atm. We have extensively tested the Durafet response in seawater using both the internal reference and a secondary Cl-ISE as a pseudo reference electrode as described above. Although the chip assembly in the Durafet is not designed for high pressure, we demonstrate a variety of applications where it shows exceptional performance at 1 atm. Our experience suggests that off-the-shelf Durafet sensors could operate up to months without calibration in shipboard laboratories and moorings in the surface ocean.

Materials and procedures

We used a Honeywell Durafet III sensor for all of the work reported here. The FET driver and pH signal conditioning electronics were furnished by either a Honeywell DL421 pH transmitter or a Honeywell Cap Adapter. An Orion Cl-ISE half cell was used as a pseudo reference electrode by direct exposure to seawater, which contains between 0.50–0.55 M Cl⁻. However, we are now making chloride ISE's in-house at MBARI, which show similar performance. We refer to these cells as the FET|INT or FET|EXT for the sensor using an internal Ag/AgCl reference and external Cl-ISE reference, respectively. Apart from the different reference electrode type, FET|INT and FET|EXT are electrically identical. The Cl-ISE is a nonporous solid made by compressing AgCl (sometimes coprecipitated with Ag_2S) into a solid pellet (Ross and Frant 1971). Both the Ag/AgCl internal reference electrode and the Cl-ISE exhibit a Nernstian response to the free chloride ion. Honeywell has already done significant work on pH and temperature calibration of the FET|INT. We have carried out similar testing in natural and artificial seawater of known pH using the FET|INT and FET|EXT and measuring both pH signals simultaneously. In both sensors the electromotive force (emf) of the cell, in this case the reference electrode-source voltage, E (Vrs in Fig. 1), follows a Nernst equation form:

$$E = E^* - S \times \log(a_H a_{Cl}) = E^* - S \times \log(\gamma_H \gamma_{Cl}) - S \times \log(m_H m_{Cl}) \quad (1)$$

where $S = R \times T \times \ln(10)/F$ (R is the gas constant 8.3145 J K⁻¹ mol⁻¹; T is temperature in Kelvin; F is the Faraday constant 96485 C mol⁻¹) and E*, similar to an electrode standard poten-

tial, is a characteristic of the two half cells forming the circuit and depends on temperature and pressure, but not on the concentration of the analyte. The reference electrode-source voltage of the cell with the internal reference also includes a liquid junction potential E_J. We chose to designate FET-based standard potentials with an asterisk rather than the conventional nought symbol (°) for reasons discussed below. In essence, the FET|EXT measures dissolved HCl directly in the sample while the FET|INT measures dissolved H⁺ in the sample and dissolved Cl⁻ in the reference gel. As the mean activity coefficient of HCl in seawater ($\gamma_\pm(HCl)^2 = \gamma_H \gamma_{Cl}$) is known through the oceans' range of temperature and salinity (Dickson 1990; Khoo et al. 1977), it is straightforward to calculate the concentration of free or total (free plus protons bound by sulfate ion) protons in seawater as the chloride ion concentration can always be obtained from salinity (Dickson et al. 2007).

Direct comparison of standard potentials of the FET|INT and FET|EXT would require an understanding of the chloride activity in the saturated KCl gel, the liquid junction potential, and how these values change with temperature. Although approximate values of KCl solubility in water are known as a function of temperature (Linke and Seidell 1965), translating this information into activities in the gel is more complicated at such high concentrations (~4.5 M KCl at 20°C). There is a sound theoretical basis for estimating a_{Cl} in the reference gel (Pitzer and Mayorga 1973), and whereas this information may provide insights into the behavior of the formal standard potential of the Durafet combination electrode, we are concerned here with performance and repeatability. Thus the theoretical aspects of the reference gel are not a primary consideration and, as is conventionally done for electrodes operating over a temperature range, the reference electrode response to a_{Cl} is incorporated into the operationally defined standard potential of the FET|INT during a calibration. In addition, liquid junction potentials are difficult to accurately quantify (Bates 1973). It is standard practice to strive to achieve identical behavior of the liquid junction in a standard relative to a sample, allowing cancellation of this term as we have done for the FET|INT. In practice, temperature-dependent terms for reference gel a_{Cl} and liquid junction potential contribute to the temperature dependence of the electrode standard potential for the FET|INT to the extent that they are repeatable. The FET|EXT has no liquid junction potential, greatly simplifying one aspect of calibration. Unlike the FET|INT, the FET|EXT does not have a repeatable a_{Cl} because the pseudo reference electrode utilizes seawater chloride ion as the reference. Fortunately, m_{Cl} is a well-defined function of salinity (Dickson et al. 2007).

The response of the FET|INT is shown in Equation 2:

$$E_{INT} = E_J + \left\{ E^*(FET|INT) - S \times \log\left[\gamma_H(sw)\right] - S \times \log\left[a_{Cl}(ref\,gel)\right] \right\} \quad (2)$$
$$- S \times \log\left(m_H\right).$$

Using a seawater calibration solution to give liquid junction potential, E_J, identical to E_J in the sample and grouping

the terms in the brackets gives pH on the concentration scale:

$$E_{INT} = E_{INT}^* - S \times \log(m_H);\qquad(3)$$

$$E_{INT}^* = \left\{ E^*(FET|INT) - S \times \log\left[\gamma_H(sw)\right] - S \times \log\left[a_{Cl}(ref\ gel)\right] \right\};\quad(4)$$

$$pH = \frac{\left(E_{INT} - E_{INT}^*\right)}{S}.\qquad(5)$$

For the FET|EXT,

$$E_{EXT} = E^*(FET|INT) - S \times \log\left(\gamma_H\gamma_{Cl}\right) - S \times \log(m_{Cl}) - S \times \log(m_H)\quad(6)$$

$$E_{EXT}^* = E^*(FET|EXT);\qquad(7)$$

$$pH = \frac{\left(E_{EXT} - E_{EXT}^*\right) + S \times \log\left(\gamma_H\gamma_{Cl}m_{Cl}\right)}{S}.\qquad(8)$$

We calculate m_{Cl} from salinity following (Dickson et al. 2007). $\gamma_H\gamma_{Cl}$ is calculated using Eq. 9 in Khoo et al. (1977) where ionic strength is calculated from salinity (Dickson et al. 2007), and the parameter A in Khoo et al. Equation 9 is approximated by fitting a second order polynomial to the data in their Table 2 to give A = $3.4286 \times 10^{-6}(T/C)^2$ + 6.7524 × $10^{-6}(T/C)$ + 4.9172×10^{-1} (R^2 = 0.99999).

Because the FET|EXT sensor is directly dependent on a_{Cl}, it is necessary to measure salinity along with FET|EXT voltage to calculate an accurate pH value. The ubiquity of salinity sensors in most autonomous sensor packages typically assures this. The approximate salinity sensitivity for the FET|EXT is 0.013 pH salinity^{-1}. Simultaneous measurement of salinity is generally carried out in most cases; for example, salinity is required for the calculation of pH in spectrophotometric pH measurements (Clayton and Byrne 1993). However, it must be noted that the FET|EXT is about 100× more sensitive to the salinity value than the spectrophotometric method or the FET|INT. On the other hand, measurement to an accuracy of 0.1 salinity, which is not a significant challenge, would supply adequate pH accuracy for most applications and in many open-ocean situations the salinity would not change by more than 0.1, further simplifying these measurements.

Typical calibration procedures for conventional pH sensors involve calibration at the measurement temperature, but many practical uses of the Durafet in oceanography will involve measurements at variable temperature. We therefore required a complete understanding of temperature impacts on sensor response. The temperature response of a pH electrode is split between the temperature dependence of the Nernst slope (R × ln(10)/F = 0.198 mV/°C) and the standard potential's function of temperature. These two temperature dependencies are sufficient to respectively describe the pH dependent and

pH independent components of the Nernst equation. All three pH independent terms in Eq. 4, including an EMF temperature coefficient for E*(FET|INT), the single ion activity coefficient of the hydrogen ion in seawater, and the reference electrode ion activity, are temperature dependent. The pH independent and temperature dependent component of E_{EXT}^* includes only an EMF temperature coefficient (Eq. 7). The technical literature is replete with standard potential values usually reported at 25°C. ISFET-based pH electrodes have a more complex standard potential function. In addition to reference electrode contributions to standard potential, the field effect transistor is a significant contributor to standard potential. By design, field effect transistors may be powered from positive or negative power supplies usually referred to as n or p channel FETs, respectively. Within these two types, operating voltages and temperature coefficients may substantially vary depending on design and semiconductor processing controls. Given these factors alone, standard potentials can be expected to vary over many volts depending on FET type, design, and processing. At this time, standard FET potentials are not portable; namely, significantly different standard FET potential values may be obtained for different FET types and for different units within the same type. The good news is that individual ISFETs provide stable and repeatable performance at constant and varying temperature, consistent with Nernstian behavior. To distinguish ISFET-based standard potentials from conventional values, the E* designation is used, as described above.

Using the temperature-dependent function of a standard seawater buffer solution to calculate the pH of the buffer (on the total hydrogen ion concentration scale) at temperature T, $pH_S(T)$, the values of standard potential at T, E*(T) are calculated over a range of temperature by measuring cell EMF at T, $E_{INT}(T)$, and $E_{EXT}(T)$:

$$E_{INT}^*(T) = E_{INT}(T) - S \times pH_S(T);\qquad(9)$$

$$E_{EXT}^*(T) = E_{EXT}(T) - S \times pH_S(T) + S \times \log(\gamma_H\gamma_{Cl}m_{Cl})(T).\qquad(10)$$

A potentially confusing aspect of using a pseudo reference electrode in a changing reference medium is placement of the terms m_{Cl} and γ_{Cl} in Eqs. 6 and 8. As discussed above, sensors based on internal reference electrodes allow inclusion of these terms in the standard potential as we have done in Eq. 4. In the case of the FET|EXT, this approach is not possible because chloride activity in the ocean is a function of temperature and salinity, and therefore, must be estimated from temperature and salinity measurement for inclusion in the pH calculation.

One characteristic of the Durafet is a well-defined, linear, and repeatable standard potential that is a simple function of temperature (Connery et al. 1992). As described above, because standard potential value is so strongly device dependent, each production Durafet is temperature tested at the factory and, based on test results, is properly temperature com-

pensated. This information, unique to each sensor and necessary to perform temperature compensation, is embedded within each sensor housing. Several Honeywell readout devices can be used to perform automatic temperature compensation for the Durafet signal of the FET|INT, which fundamentally consists of accounting for the temperature dependence of the standard potential (Connery and Shaffer 1989). Provision for device-specific temperature dependence makes the Durafet particularly easy to use in many cases. Shipboard underway measurements, for example, are relatively straightforward to set up when using the temperature compensated output of the DL421-Durafet combination, as we have done. The 4-20 mA output of the DL421 can be recorded on a variety of A/D converters connected to a PC.

Operating a Durafet in a fully autonomous setting that demands low power consumption is slightly more complicated. The sensor and readout electronics combination requires 1 h warm-up so, for measurements on moorings or other platforms designed to observe rapidly changing pH, the FET must remain continuously powered. Although the chip operates at < 200 µA, the DL421 will drain batteries in a short period. The alternative is to use the Honeywell Cap Adapter, which is an analog preamplifier and power supply for the FET. The Cap Adapter supplies the raw pH signal (biased to ~0 V at pH = 7 for the FET|INT), without temperature compensation. The Cap Adapter and Durafet combination requires approximately 2 mW to operate continuously. We used the Cap Adapter-Durafet combination in a battery-powered autonomous sensor. Because the Cap Adapter does not perform temperature compensation and because we used a secondary reference electrode with different temperature dependence, it was necessary to design our own setup using automated temperature cycling to determine the temperature dependence of E^*. This was carried out in a 5 L jacketed beaker with a custom built airtight lid. The beaker was filled with the buffer 2-amino-2-hydroxymethyl-1,3-propanediol (TRIS, nominal pH ~8.1) or the buffer 2-aminopyridine (AMP, nominal pH ~6.8). Equimolar amounts of the acid and base forms of the buffers in synthetic seawater were used (Dickson 1993b). The pH of an equimolar TRIS or AMP buffer equals the pK_a of the acid form of the respective buffer, which is well defined as a function of temperature (Dickson 1993b). We recorded the FET|INT and FET|EXT signal as temperature was repeatedly cycled between 5 to 35°C. A typical temperature cycling test consisted of seven temperature steps from 5 to 35°C using 2–6 h interval per step. In a single test, data were recorded continuously for several days. These measurements were used to determine E^* as a linear function of temperature using Eq. 9 and Eq. 10.

pH response (i.e., Nernst slope) was initially verified over the seawater range using secondary standards. The standards were prepared by spiking sterilized seawater with small amounts of 0.1 M HCl or 0.05 M Na_2CO_3 and sparging the solutions with ambient air to stabilize CO_2. pH values were then assigned to each calibration solution after analysis using

typical spectrophotometric pH procedures (Clayton and Byrne 1993). The Nernst slope was then repeatedly and, we believe, more accurately verified by comparing the sensor response in TRIS to that in AMP. These comparisons were made for each of the seven temperature steps described above. For Nernstian behavior, we compared voltages recorded in TRIS versus AMP solutions with added Br⁻ to represent seawater. Measurements are compared after a short conditioning period in which the ISE is allowed to come to equilibrium with Br⁻. The Percent Theoretical Slope (PTS) is calculated as

$$PTS = \frac{\left[E(T_1, pH_1) - E^*(T_1)\right] - \left[E(T_2, pH_2) - E^*(T_2)\right]}{pH_1 \times T_1 - pH_2 \times T_2} \times \frac{F}{R \times \ln(10)} \quad (11)$$

where subscripts represent two buffer solutions of appreciably different pH (i.e., TRIS and AMP) and the temperatures at which the two buffers are measured. Although Eq. 11 can be used for measurements of any two buffers at different temperatures, to minimize the contribution of errors in the slope of $E^*(T)$, we only calculated PTS for corresponding temperature steps in TRIS and AMP where the temperature differences during measurement of E were always less than 0.13°C, leading to near negligible contributions from the $E^*(T)$ terms in Eq. 11.

In July 2007, a Durafet connected to a DL421 was installed on the underway line of MBARI's ship, the Western Flyer. In addition to pH, partial pressure of carbon dioxide (pCO_2) and total dissolved inorganic carbon (TCO_2) were measured on the same underway line using instrumentation developed at MBARI by Gernot Friederich based on nondispersive infrared analyzers (Friederich et al. 2002).

In December 2008, a Durafet and a Cl-ISE were immersed in the 1,420,000 L (375,000 gal) MBARI test tank (filtered and sterilized seawater) at a depth of ~2 m. The output signal from the FET|INT and FET|EXT were recorded continuously by a 24-bit A/D voltage converter connected to a PC. Because it is indoor and ventilated, the MBARI seawater tank is normally very stable with respect to both temperature and pH. However, in the fall of 2008, the tank was refilled with new seawater that was not fully equilibrated with the atmosphere. Because the tank is only slowly mixed, gas equilibration was very slow following the refilling, taking several months with pH drifting upwards nearly constantly as CO_2 outgassed. This provided an excellent situation for testing stability and drift of the sensor over a range of pH. At the time of writing, we have now collected 7 months of continuous pH in the test tank without any servicing of the sensor and with regular bottle samples for spectrophotometric pH measurement.

MBARI maintains a number of moorings in Monterey Bay. Twin autonomous versions of the Durafet were deployed for 2 months in the surface ocean on the M0 mooring, located about 5 km from shore near the center of the Bay. This first version of the autonomous Durafet consists of 4 alkaline D-cell batteries, a CF2 datalogger (Persistor) with a 24 bit A/D converter (Oceanographic Embedded Systems), Omega PHTX-21 unity gain pre-

amp for the FET|EXT, custom analog board, and pressure housing. The Cap Adapter was continuously powered from a ± 3.3V supply on the analog board. The analog board was also used to switch power to voltage dividers to monitor temperature from the Durafet's internal thermistor and battery voltage.

Assessment

Figure 2 shows the output of both common Durafet readout electronics over the seawater pH range in natural seawater, which has been slightly perturbed to form these secondary standards. We repeatedly tested Durafet sensors in TRIS and AMP and consider these results to be most reliable for assessing the Nernst slope (*see* below). The slope of the least squares line for the secondary standards was slightly low (57 mV/pH corresponding to 98% of the expected Nernst slope). This was probably due to errors in our knowledge of the pH of the secondary standards and the fact that these solutions are not very stable over time because they are only weakly buffered by carbonate equilibria at near-seawater concentrations and may have changed slightly between spectrophotometric analyses and electrode measurement. Sandifer and Voycheck (1999) found that the Nernst slope of the Durafet held constant over 3 months (within the resolution of their measurements). We verified Nernstian behavior by comparing results of temperature cycling tests, but have not yet tested for changes in the pH response slope over several months as done by Sandifer and Voycheck (1999). Using data over the full temperature range 5 to 35°C (same data discussed below in Table 1), we calculated $PTS_{INT} = 99.5 \pm 0.7\%$ and $PTS_{EXT} = 98.6 \pm 0.3\%$. These slightly low values may again reflect small errors in our knowledge of the buffer composition (*see* below for more discussion on this issue). In the future, we plan to prepare the large batches of TRIS and AMP required for these tests to a higher degree of accuracy.

Temperature cycling tests have been carried out on several different Durafet sensors. Figure 3 shows the results recorded during one of the 10 days series of cycles from 5 to 35°C. In Fig. 3, the term V_{out} is used in place of E_{INT} because the Cap Adapter applies a voltage bias (mentioned above) on the order of ~1 V so that $V_{out} = E_{INT} + V_{bias}$. The Cap Adapter V_{out} provides exactly the same information as E_{INT}; the voltage bias is necessary for a Cap Adapter-Durafet combination to function universally on all pH meters. The temperature and pH signal, V_{out}, shown in Fig. 3A are filtered to provide a single average point at the end of each temperature step. Fig. 3B shows the standard deviations of 2-h averages for both temperature and V_{out} at the end of each step in Fig. 3A. In our system, the stability of V_{out} is somewhat related to temperature variability, which roughly doubles from ± 0.01°C at 20°C (i.e., near room temperature) to 0.02°C at 5 and 35°C. Temperature control could be improved using a better insulated system, but we have found this setup to be adequate for the assessment here.

We compiled a set of 25 temperature steps in TRIS and AMP at the seven different temperatures, consisting of 50 discrete measurements over the temperature range. These data were
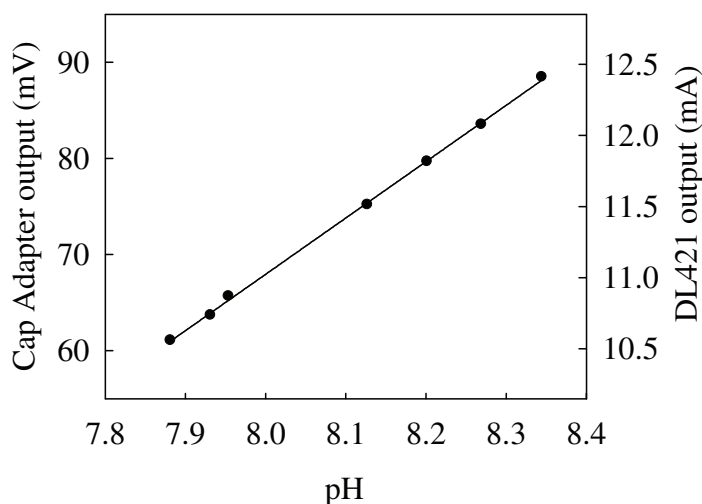

Fig. 2. Initial seawater pH calibrations for the Durafet were carried out using secondary standards prepared from seawater and determined using spectrophotometric methods, as described in the text.
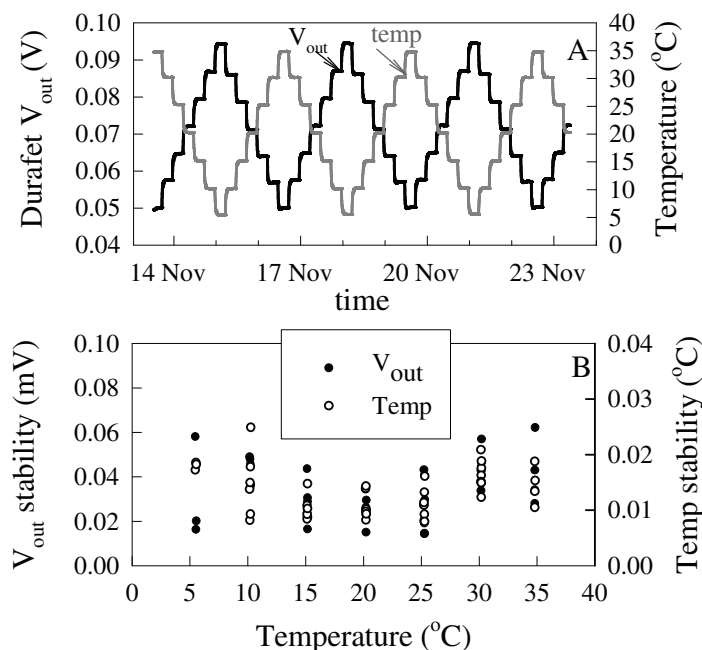

Fig. 3. Temperature cycling of a Durafet in a seawater Tris buffer. (A) Temperature and Cap Adapter output voltage (V_{out}) and (B) the 1σ standard deviation of temperature and V_{out} for the last 2 h of each time step.

collected similar to the cycling test described above but not always in the exact same order of temperature steps and sometimes with shorter intervals of 2 h per step instead of 6 h per step. Fitting linear trend lines to this data, we calculated the slope for E^* versus temperature for a single ISFET operating with both reference electrodes (Table 1).

In these and additional tests, we never found an improvement in R^2 values when using higher-order polynomials to fit

Table 1. Temperature dependence of standard potentials.

Parameter	Description	TRIS	AMP
$\partial E^*_{EXT}/\partial T$	Function of a_H(sample) and a_{Cl}(sample) (Eq. 10)	-1.081 ± 0.004 mV°C^{-1} ($R^2 = 0.9994$)	-1.066 ± 0.005 mV°C^{-1} ($R^2 = 0.9994$)
$\partial E^*_{INT}/\partial T$	Function of a_H(sample) (Eq. 9)	-1.455 ± 0.011 mV°C^{-1} ($R^2 = 0.9980$)	-1.456 ± 0.014 mV°C^{-1} ($R^2 = 0.9979$)
$\partial E^*_{INT}/\partial T$	Function of a_H(sample) and a_{Cl}(gel) (Eq. 10)	-1.101 ± 0.011 mV°C^{-1} ($R^2 = 0.9966$)	-1.102 ± 0.014 mV°C^{-1} ($R^2 = 0.9965$)

E^* to temperature and conclude that, for both FET|INT and FET|EXT, E^* is a linear function of temperature. We did find that, when using longer temperature equilibration steps of 6 h rather than mixed times consisting mostly of shorter steps, the R^2 values of the linear trend lines were higher (e.g., for $\partial E^*_{INT}/\partial T$ in TRIS, we obtained $R^2 = 0.9996$ and 0.9980 using points at the end of 6 h time steps and mostly 2 h time steps, respectively). Intercepts are not provided with the slopes reported in Table 1 because, as discussed earlier, E^* varies widely with each particular device. The first two rows of Table 1 represent the values calculated for the FET|INT and FET|EXT using Eq. 9 and Eq. 10, respectively. The third row reports values for the FET|INT when we attempt to calculate E^*_{INT} using an equation identical to Eq. 10, but where a_{Cl} is estimated for the reference gel. As discussed earlier, it is more practical to use Eq. 9 to calculate $\partial E^*_{INT}/\partial T$. Row 3 in Table 1 is provided because these values are directly comparable to those in Row 1. It is quite encouraging that these numbers agree to within ~30 µV°C^{-1}. The small difference is attributable to insufficient knowledge of a_{Cl} in the reference gel. We have not performed such comprehensive temperature cycling tests on different sensors, but based on several shorter tests, it is clear that the $\partial E^*/\partial T$ value is much more consistent between different sensors. For this reason, we report one set of values in Table 1 to illustrate the temperature response of the sensor. However, until more data are documented we recommend similar calibration for each sensor for the most accurate work.

E^*_{EXT} values for a temperature cycling test in TRIS (Table 1), calculated using Eq. 10, and their corresponding residuals for a linear fit are shown in Fig. 4. The majority of error at each temperature step is due to a very small but measurable hysteresis effect that led to an observed pH up to ~0.003 pH units greater during temperature down-cycling, as opposed to up-cycling Fig. 4B. This hysteresis was greatest at 20°C and minimal at 5°C and 35°C. The hysteresis observed likely results from two effects. First, the internal temperature sensor and the gel-filled KCl reference electrode lag the actual temperature of the solution because of the thermal mass of the Durafet. However, the FET surface appears to be in near equilibrium with the solution temperature. We can correct for the thermal lags mathematically or by only using data when the sensor system has been at equilibrium for several tens of minutes. The second source of hysteresis is unknown, but may result from slow re-equilibration of the AgCl in the electrode boundary layer to reach a new equilibrium value. The fact that we are even able to detect such an extremely small hysteresis is a testament to the sensor's stability.
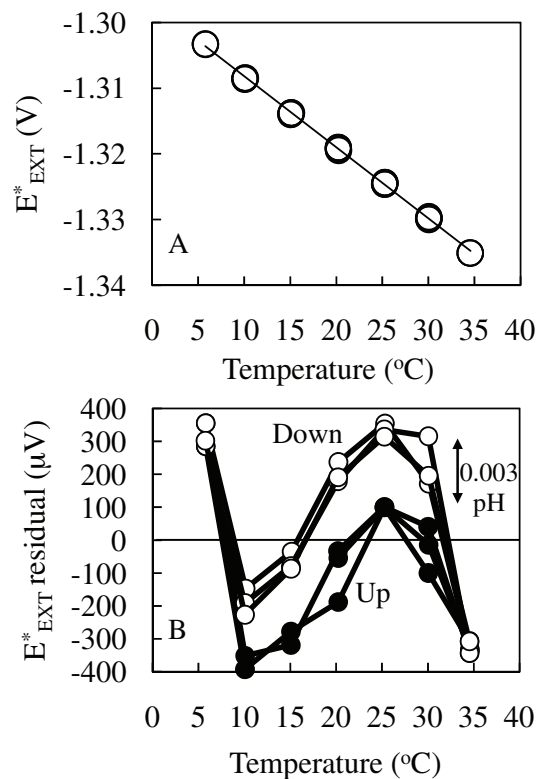

Fig. 4. (A) Standard potential of a FET|EXT calculated using Eq. 10; same data used to calculate $\partial E^*_{EXT}/\partial T$ for TRIS in Table 1. (B) Residuals from the linear fit shown in panel A. Sensors were operated using a Cap Adapter and voltages were recorded using a National Instruments 9219.

Underlying the hysteresis is a systematic error for both sensors' E^*, apparent as a sine-shape curve in Fig. 4B. The systematic errors in E^* may arise from several sources. E^* may deviate from a linear function of temperature (Bates 1973), although as stated above we do not believe that this is the case. An error in buffer composition would also contribute to the systematic deviations (*not* the hysteresis) as pH would no longer equal pK_a. If the buffer is not prepared in an exactly equimolar ratio, then pH of the solution will deviate by a different amount, depending on temperature, from the equation used to calculate TRIS pH (Dickson 1993b). We have observed a deviant pH versus temperature relationship between a previous batch of TRIS (measured spectrophotometrically at different temperatures) and the equation published by Dickson (1993b), amounting to pH errors up to 0.01. We attributed this to errors in our buffer preparation. We believe that the systematic errors

observed for E* are a result of errors in buffer preparation, as we did not prepare TRIS solutions with the same degree of accuracy described by Dickson, but postcalibrated the TRIS pH using a spectrophotometric measurement at 20°C. Although this approach may be satisfactory if measurements are always preformed near 20°C, the results shown in Fig. 4 indicate that accurate temperature calibration over the full seawater range of temperatures will require highly accurate pH buffer solutions. This underscores the great need for a centralized preparation-standardization-distribution program of seawater pH buffers, similar to the widely used CO_2 Certified Reference Materials (Dickson 2001).

Most temperature cycling experiments were carried out with a Cap Adapter rather than a DL421 because our main goal was to develop an autonomous sensor based on the Cap Adapter. As mentioned above, the DL421 output is compensated to correct for changes in E_{INT}^*, giving a signal directly proportional to pH over a range of temperature. In early tests, we verified this by recording DL421 output in a TRIS solution during temperature cycling. We calculated pH errors for the DL421 by changing the DL421 4 to 20 mA output to pH units and then subtracting the known pH of the TRIS solution at each temperature point from the DL421 output value. This technique produced a set of residuals closely resembling Fig. 4B (data not shown) with similar magnitudes of error in pH units, indicating that Honeywell's temperature compensation is accurate because we assume that the systematic errors observed in both Cap Adapter and DL421 residual plots are due to our buffer composition as described above.

Over 6 months in the MBARI test tank, both FET|INT and FET|EXT registered little or no detectable drift (Fig. 5). As described above, the primary trend seen in the pH data is due to CO_2 outgassing from the 10 m deep tank. Smaller negative excursions in pH, such as the one in late February, occurred during testing of MBARI FOCE (Free Ocean CO_2 Experiment) equipment, which releases CO_2 into the water. Negative spikes in the pH signal occur when air bubbles (replete in the tank due to frequent ozonation) attach to the surface of the FET. Comparison of Fig. 5B to Fig. 5C indicates that in a natural seawater environment free of biofouling (i.e., the MBARI test tank), FET|EXT is the more stable sensor. Taking the difference of the two sensor signals to remove the ISFET component can be used to extract the signal of the two reference electrodes: INT|EXT (Fig. 5D). This reveals a significant drift between the two reference electrodes during the first 1.5 months of the test tank deployment. Comparison with the spectrophotometric data (Fig. 5B and C) indicates that the 1.5 months of drift originates in the FET|INT sensor. Appreciation of these artifacts suggests that the Durafet is capable of measuring pH with a precision better than 0.005 over periods in excess of a month, but may require a conditioning period.

Fig. 6 presents pH and pCO_2 during one leg of a cruise from 36.74°N 122.02°W (Monterey Bay) to 33.29°N 129.43°W (~670 km southwest of Monterey Bay, across the California Current
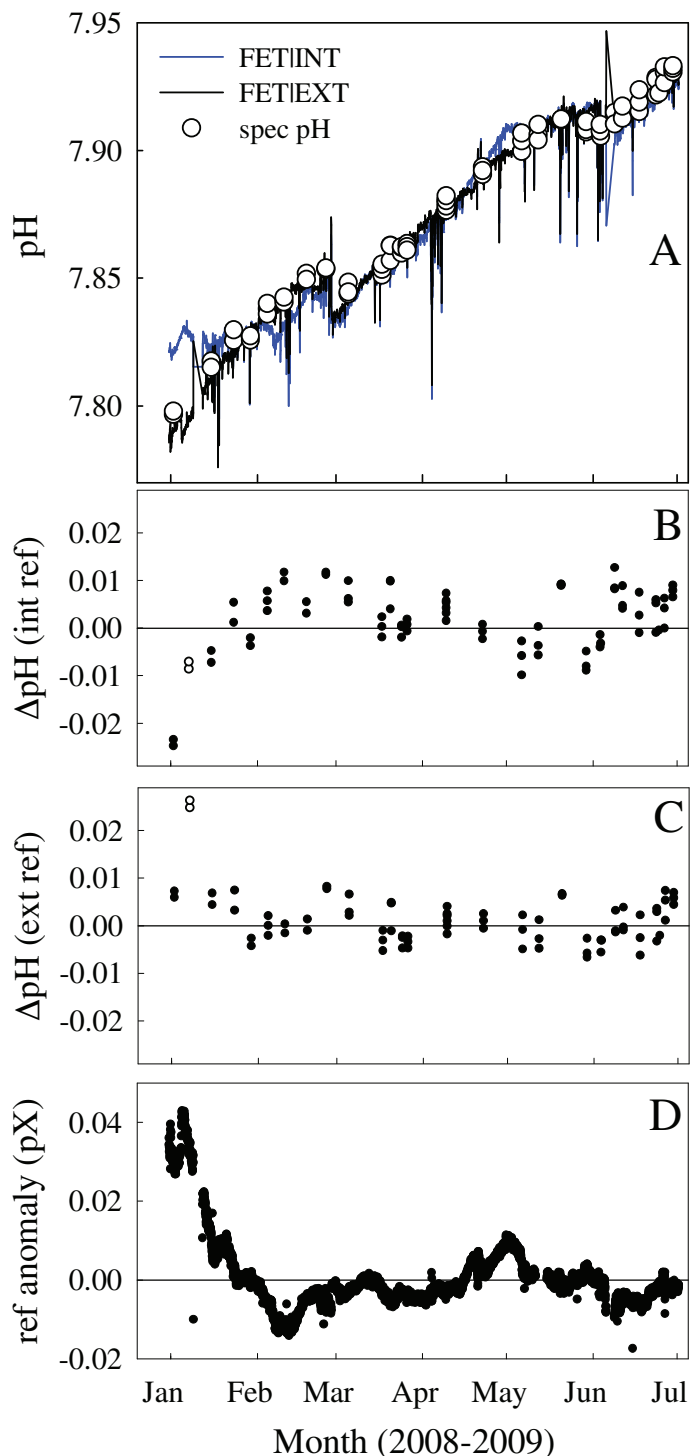

Fig. 5. (A) Six months of continuous operation in the MBARI test tank for a single Durafet using both the internal reference electrode and an external Cl-ISE. Discrete samples were collected by bottle and measured using standard spectrophotometric pH protocols. (B) and (C) show residuals between the sensor and discrete measurements for the internal and external reference electrodes, respectively. (D) The difference between the two reference half cells, attributed mostly to drift in the liquid junction potential. Sensors were operated using a Cap Adapter and voltages were recorded using a National Instruments 9219.
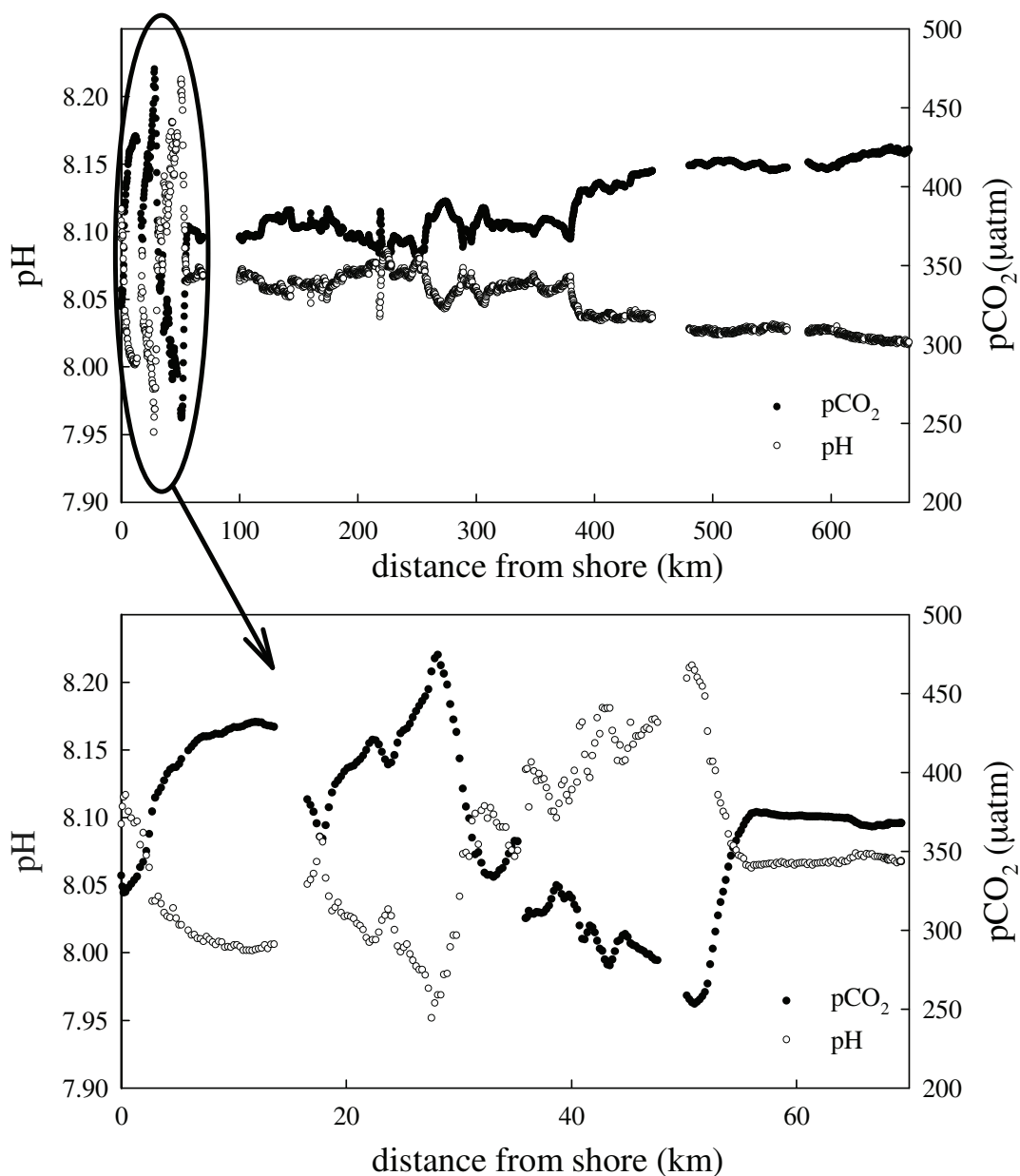
Fig. 6. Underway data from a cruise in the eastern North Pacific off the central California coast in July 2007. Distance 0 km is 36.74°N 122.02°W (Monterey Bay) and distance 670 km is 33.29°N 129.43°W. The bottom panel shows an enlarged view of the 0–70 km nearest the shore. pCO_2 data provided by Gernot Friederich.

transition zone into North Pacific Gyre water). Pronounced near-shore variability is due to biological activity, upwelling of high CO_2 water, and mixing of the different water masses. pH closely mirrors pCO_2, as expected (Fig. 7). The very tight relationship over the entire transect shown in Fig. 6 indicates that the ISFET performs satisfactorily over a range of pH, temperature, and salinity (pH = 7.9–8.3; temp = 12 to 20°C; salinity = 32.4–33.8). Also shown in Fig. 7 is pH calculated from pCO_2 and TCO_2. During this cruise, the pCO_2 and TCO_2 systems were periodically recalibrated with standard gases (NIST) and certified reference materials (Dickson 2001), respectively. The

Durafet measurement was calibrated at the beginning of the cruise by adjusting its readout to agree with pH calculated from the pCO_2 and TCO_2 systems (on the "total" hydrogen ion concentration scale), and then the pH sensor was not serviced for the remainder of the cruise. Increased scatter in Fig. 7 may be partly due to air bubbles landing on the FET in the underway line. As discussed below, because the Durafet signal can be rapidly recorded and averaged, signal averaging can reduce the scatter in Fig. 7 to a value similar to that obtained by the underway TCO_2-pCO_2 system. Although Fig. 6 and Fig. 7 present only a single transect, the Durafet performed with
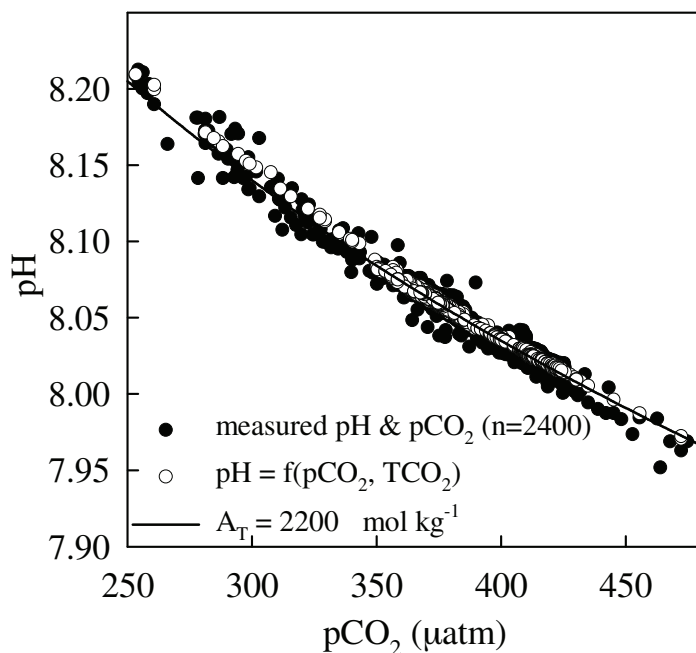
Fig. 7. Relationship between underway ISFET pH and LICOR pCO_2 shown in Fig. 6. Also shown is pH calculated using underway TCO_2 and pCO_2. The line represents the conservative relationship between pH and pCO_2 for A_T = 2200. Underway pCO_2 and TCO_2 provided by Gernot Friederich.

similar precision and stability on the return cruise and on a repeat cruise in October. This again demonstrates the potentially high stability of ISFET sensors under conditions where repeat calibration is not possible. As discussed above, calibration procedures based on seawater buffer solutions are available. In the future, an accurately calibrated pH sensor will provide a third CO_2 variable to this underway system. Such "overdetermination" of the CO_2 system is useful for studying the internal consistency and testing our current knowledge of seawater CO_2 thermodynamics (Lueker et al. 2000).

The short-term performance of the ISFET is assessed using underway data where the distance from shore is greater than 600 km (Fig. 8, Fig. 9). TCO_2, calculated from pH and pCO_2, is also shown for reference (Fig. 8). We note that, while the combination of pH and pCO_2 is not preferred for calculation of TCO_2 (Millero 2007), in the example given here it is useful for framing the short-term precision of the measurements in terms of µmol kg^{-1} inorganic carbon. Over ~65 km, where TCO_2 is nearly constant (> 600 km from shore, Fig. 8), the 1σ standard deviation in TCO_2 derived from pH and pCO_2 is 5.5 µmol kg^{-1} (n = 245), or 3.5 µmol kg^{-1} when binned on 5 min intervals to match the measurement frequency of the TCO_2 analyzer, which gave a corresponding precision of 3.0 µmol kg^{-1} (*n* = 88). Over the narrow range of pCO_2 (412–425 µatm) found in water > 600 km from shore, the relationship between pH and pCO_2 is linear within the accuracy of the measurements. Treating these data as purely linear, we performed
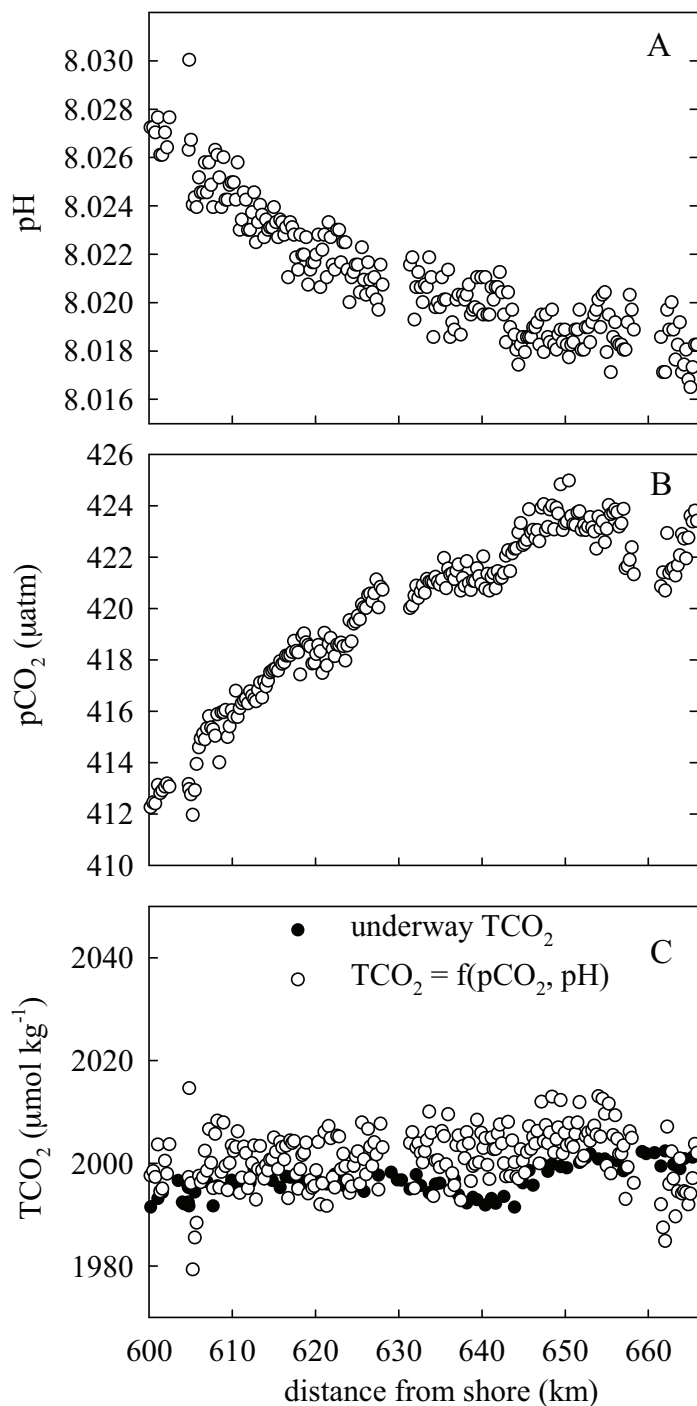

Fig. 8. Underway pH (A) and pCO_2 (B) data from Fig. 6, limited to offshore measurements greater than 600 km from shore. TCO_2 (C) is also shown for reference.

a Model II least squares regression of pH versus pCO_2 (Fig. 9). The bottom panel in Fig. 9 shows the Model II residuals of pH, which have 1σ = 0.0010 pH unit (*n* = 245) over 5 h.

Results from 2 months of continuous operation on the Monterey Bay M0 mooring indicate that the Durafet is
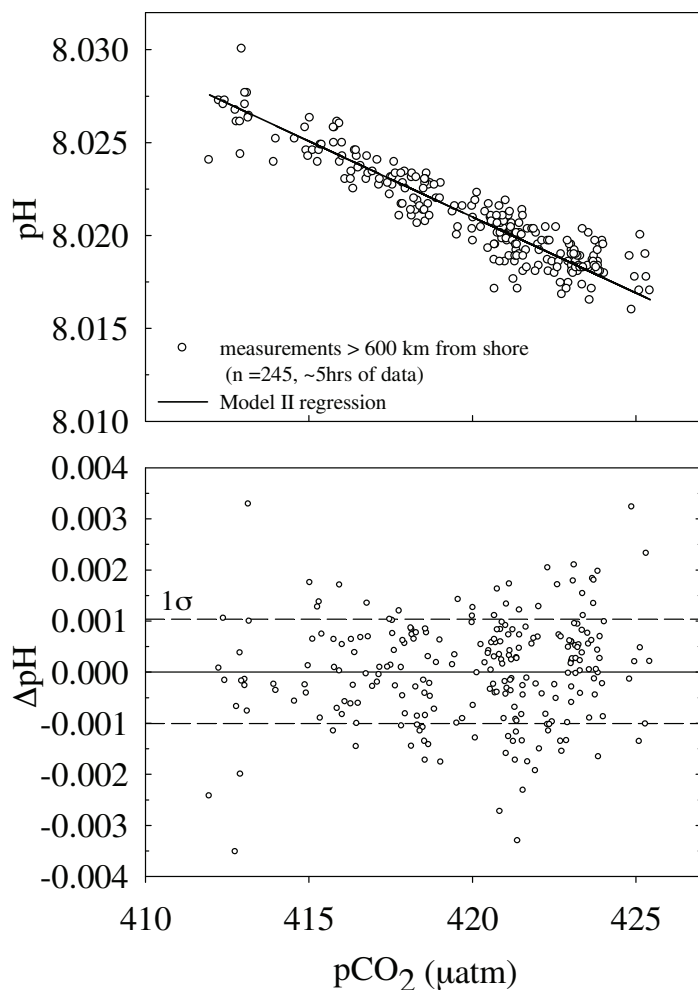
Fig. 9. Offshore data greater than 600 km (same data as shown in Fig. 8). Over this narrow range of values, pH and pCO_2 are essentially linear and the deviation from a Model II regression line is used to examine the short-term stability of the ISFET.

quite robust over extended periods (Fig. 10). Plotting the M0 pH versus pCO_2 data (Fig. 10A) produces a figure (not shown) very similar to Fig. 7 with a tight relationship between all four signals (two FET|INT and two FET|EXT) with the pCO_2 sensor. The agreement between the different pH signals was generally around 0.01 pH units or better, which easily resolved diel cycling and upwelling signals with resolution similar to the pCO_2 sensor. M0 is located in a high fouling (coastal upwelling) environment. Based on a comparison of long-term sensor performance in the absence of biofouling (Fig. 5), we attribute the majority of excursions seen in the sensor 1 versus sensor 2 pH anomaly (Fig. 10B) to biofouling. We are currently designing different flow-through manifolds for the Durafet that can be attached to pumped sample circuits. Under the circumstances, the data shown in Fig. 10 are extremely encourag-

ing, as the sensors were only minimally protected by coarsely perforated copper.

Comments and recommendations

Recent progress in industrial pH sensor technology now provides new methods of mapping large-scale features of the oceanic carbon dioxide system. pH can be used in combination with another CO_2 parameter (i.e., pCO_2, total dissolved inorganic carbon, or total alkalinity) to characterize the aqueous CO_2 system. Our preliminary data suggest that underway ISFET pH would be a suitable parameter for surface mapping from, for example, research vessels and volunteer observing ships.

ISFET-based pH sensors generally exhibit response times on the order of milliseconds. The channel insulator and substrate comprising the solid-state FET are intrinsically insensitive to pressure. These characteristics (fast response time and high pressure tolerance) make the ISFET an excellent candidate for profiling applications on robotic floats/gliders, AUVs, ROVs, and CTDs in addition to providing exciting new possibilities such as eddy correlation for quantifying the inorganic carbon flux across the sediment-water interface. However, we have found during attempts to build a pressure tolerant pH sensor that mechanical strain on the entire chip can produce a pressure dependent output signal. We are exploring novel methods of chip encapsulation to eliminate this signal, while still retaining the excellent long-term stability found in the current implementation of the Durafet. Shitashima's novel use of the Cl-ISE as a reference electrode has already led to a variety of pH measurements at high pressure from ROVs (Shitashima et al. 2008). This would eliminate potential problems with pressure- and temperature-induced changes in liquid junction potentials that may exacerbate hysteresis during temperature cycles (note that we observed a greater hysteresis effect for the FET|INT opposed to the FET|EXT). One of our future goals is pH measurement from profiling floats, which are a very promising platform for deployment of biogeochemical sensors (Bishop et al. 2004; Körtzinger et al. 2004; Riser and Johnson 2008).

Encapsulation of the ISFET chip to protect the signal conditioning electronics, while still exposing the channel insulator, has been one of the limitations of ISFET technology (Oelßner et al. 2005). In particular, exposing ISFETs to high pressure over long periods and repeated T-P cycles while maintaining high resistance in the encapsulation is a significant challenge. Chips with high pressure tolerance have been built in-house by experts (e.g., Shitashima et al. 2002), but to our knowledge no commercially available ISFET is sufficiently pressure tolerant to be used in the deep ocean. MBARI and SIO are currently working with Honeywell to develop such a device, which would be available to the greater oceanographic community. We plan a later report on the necessary procedures related to calibration and pH calculation for this device.
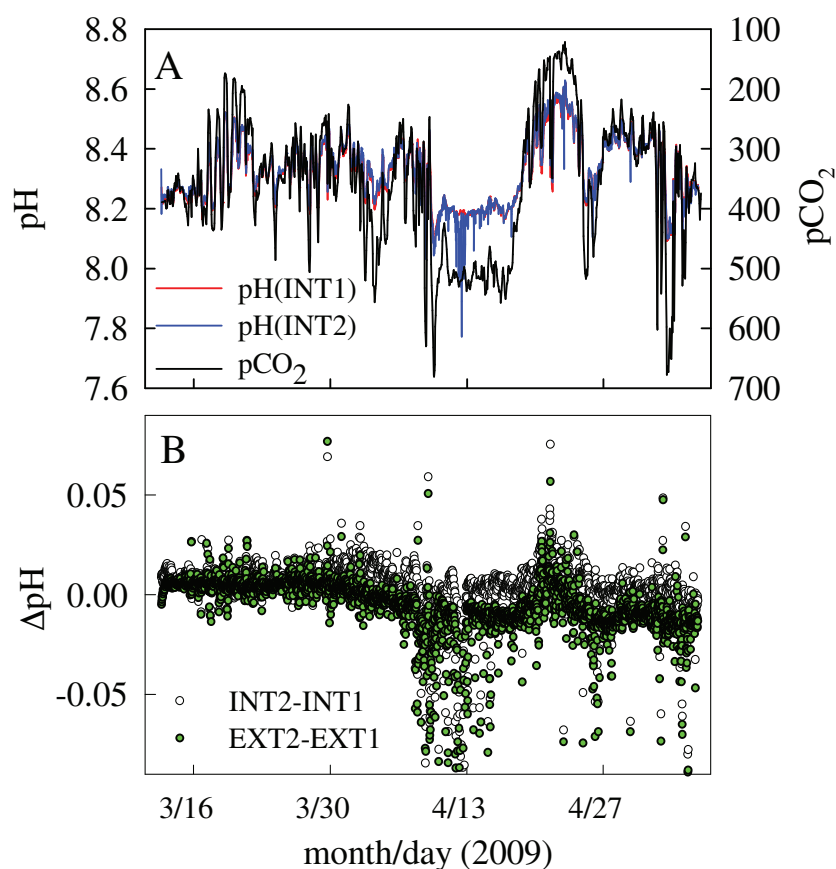
Fig. 10. Two months of pH sensor data from dual pH sensors deployed on the Monterey Bay M0 mooring. (A) pH from the two durafets using internal references (int) and pCO_2 (right axis, inverted). (B) Differences in pH between the two sensors measured by both internal and external reference (ext) electrodes.

References

Bates, R. G. 1973. Determination of pH: Theory and practice, 2nd ed. Wiley.

Bellerby, R. G. J., A. Olsen, T. Johannessen, and P. Croot. 2002. A high precision spectrophotometric method for on-line shipboard seawater pH measurements: the automated marine pH sensor (AMpS). Talanta 56:61-69 [doi:10.1016/S0039-9140(01)00541-0].

Bergveld, P. 2003. Thirty years of ISFETOLOGY. What happened in the past 30 years and what may happen in the next 30 years. Sens. Actuators B Chem. 88:1-20 [doi:10.1016/S0925-4005(02)00301-5].

Bishop, J. K. B., T. J. Wood, R. E. Davis, and J. T. Sherman. 2004. Robotic observations of enhanced carbon biomass and export at 55°S during SOFeX. Science 304:417-420 [doi:10.1126/science.1087717].

Clayton, T. D., and R. H. Byrne. 1993. Spectrophotometric seawater pH measurements: total hydrogen ion concentration scale calibration of m-cresol purple and at-sea results. Deep-Sea Res. I 40:2115-2129 [doi:10.1016/0967-0637(93)90048-8].

Connery, J. G., and E. W. Shaffer, Jr.; inventors; General Signal Corporation; assignee. Temperature compensation for potentiometrically operated ISFETs. US Patent 4,879,517. 1989 Nov 7.

———, R. D. Baxter, and C. W. Gulczynski. 1992. Development and performance characteristics of a new pH electrode. *In* Pittsburgh Conference; 1992 Mar 9–12; New Orleans. Honeywell International. Paper #561.

Culberson, C. H. 1981. Direct potentiometry. *In* M. Whitfield and D. Jagner [eds.], Marine electrochemistry. Wiley.

Dickson, A. 1990. Standard potential of the reaction: AgCl(s) + 1/2 $H_2(g)$ = Ag(s) + HCl (aq), and the standard acidity constant of the ion HSO_4^- in synthetic sea water from 273.15 to 318.15 K. J. Chem. Thermodyn. 22:113-127 [doi:10.1016/0021-9614(90)90074-Z].

———, C. L. Sabine, and J. R. Christian [eds.]. 2007. Guide to best practices for ocean CO_2 measurements. North Pacific Marine Science Orgnaizaiton (PICES). PICES special publication 3.

Dickson, A. G. 1993a. The measurement of seawater pH. Mar. Chem. 44:131-142 [doi:10.1016/0304-4203(93)90198-W].

———. 1993b. pH buffers for sea water media based on the total hydrogen ion concentration scale. Deep Sea Res. I 40:107-118 [doi:10.1016/0967-0637(93)90055-8].

———. 2001. Reference materials for oceanic measurements. Oceanography 14:21-22.

Ding, K., J. W. E. Seyfried, Z. Zhang, M. K. Tivey, K. L. Von Damm, and A. M. Bradley. 2005. The in situ pH of hydrothermal fluids at mid-ocean ridges. Earth Planet. Sci. Lett. 237:167-174 [doi:10.1016/j.epsl.2005.04.041].

Fabry, V., and others. 2008. Ocean acidification's effects on marine ecosystems and biogeochemistry. Eos Trans. AGU 89:15 [doi:10.1029/2008EO150004].

Feely, R. A., and others. 2004. Impact of anthropogenic CO_2 on the $CaCO_3$ system in the oceans. Science 305:362-367 [doi:10.1126/science.1097329].

Friederich, G., P. Walz, M. Burczynski, and F. Chavez. 2002. Inorganic carbon in the central California upwelling system during the 1997–1999 El Niño–La Niña event. Progr. Oceanogr. 54:185-203 [doi:10.1016/S0079-6611(02)00049-6].

Friis, K., A. Körtzinger, and D. W. R. Wallace. 2004. Spectrophotometric pH measurement in the ocean: Requirements, design, and testing of an autonomous charge-coupled device detector system. Limnol. Oceanogr. Methods 2:126-136.

Khoo, K. H., R. W. Ramette, C. H. Culberson, and R. G. Bates. 1977. Determination of hydrogen ion concentrations in seawater from 5 to 40°C: standard potentials at salinities from 20 to 45%. Anal. Chem. 49:29-34 [doi:10.1021/ac50009a016].

Kleypas, J. A., R. A. Feely, V. J. Fabry, C. Langdon, C. L. Sabine, and L. L. Robbins. 2006. Impacts of ocean acidification on coral reefs and other marine calcifiers: a guide for future research, report of a workshop held 18–20 April 2005, St. Petersburg, FL, sponsored by NSF, NOAA, and the U.S. Geological Survey. <http://www.pmel.noaa.gov/co2/>.

Körtzinger, A., J. Schimanski, U. Send, and D. Wallace. 2004. The ocean takes a deep breath. Science 306:1337 [doi:10.1126/science.1102557].

Le Bris, N., and D. Birot. 1997. Automated pH-ISFET measurements under hydrostatic pressure for marine monitoring application. Anal. Chim. Acta 356:205-215 [doi:10.1016/S0003-2670(97)00533-3].

Linke, W. F., and A. Seidell. 1965. Solubilities inorganic and metal-organic compounds. V. 2. American Chemical Society.

Liu, X., Z. A. Wang, R. H. Byrne, E. A. Kaltenbacher, and R. E. Bernstein. 2006. Spectrophotometric measurements of pH in-situ: Laboratory and field evaluations of instrumental performance. Environ. Sci. Technol. 40:5036-5044 [doi:10.1021/es0601843].

Lueker, T. J., A. G. Dickson, and C. D. Keeling. 2000. Ocean pCO_2 calculated from dissolved inorganic carbon, alkalinity, and equations for K1 and K2: validation based on laboratory measurements of CO_2 in gas and seawater at equilibrium. Mar. Chem. 70:105-119 [doi:10.1016/S0304-4203(00)00022-0].

Martz, T. R., J. J. Carr, C. R. French, and M. D. Degrandpre. 2003. A submersible autonomous sensor for spectrophotometric pH measurements of natural waters. Anal. Chem. 75:1844-1850 [doi:10.1021/ac020568l].

Millero, F. J. 2007. The marine inorganic carbon cycle. Chem. Rev. 107:308-341 [doi:10.1021/cr0503557].

Nakano, Y., H. Kimoto, S. Watanabe, K. Harada, and Y. Watanabe.

2006. Simultaneous vertical measurements of in situ pH and CO_2 in the sea using spectrophotometric profilers. J. Oceanogr. 62:71-81 [doi:10.1007/s10872-006-0033-y].

Oelßner, W., and others. 2005. Encapsulation of ISFET sensor chips. Sens. Actuators B B105:104-117 [doi:10.1016/S0925-4005(04)00374-0].

Pitzer, K. S., and G. Mayorga. 1973. Thermodynamics of electrolytes. II. Activity and osmotic coefficients for strong electrolytes with one or both ions univalent. J. Phys. Chem. 77:2300-2308 [doi:10.1021/j100638a009].

Raven, J., and others. 2005. Ocean acidification due to increasing atmospheric carbon dioxide. The Royal Society.

Riser, S. C., and K. S. Johnson. 2008. Net production of oxygen in the subtropical ocean. Nature 451:323-325 [doi:10.1038/nature06441].

Ross, J. W., M. S. Frant, and J. H. Riseman, inventors; Orion Research, assignee. Halide-sensitive electrochemical electrodes and method of making same. US patent 3,563,874. 1971 Feb 16.

Sabine, C. L., and others. 2004. The oceanic sink for anthropogenic CO_2. Science 305:367-371 [doi:10.1126/science.1097403].

Sandifer, J., and J. Voycheck. 1999. A review of biosensor and industrial applications of pH-ISFETs and an evaluation of Honeywell's "DuraFET." Microchim. Acta 131:91-98 [doi:10.1007/s006040050013].

Schubert, R. 2006. The future oceans warming up, rising high, turning sour: Summary for policy makers. German Advisory Council on Global Change (WBGU).

Sedjil, M., G. N. Lu, G. Michard, and F. Prevot. 1998. A colorimetric method with the use of BDJ detector for seawater pH measurement. Anal. Chim. Acta 377:179-184 [doi:10.1016/S0003-2670(98)00525-X].

Seidel, M. P., M. D. Degrandpre, and A. G. Dickson. 2008. A sensor for in situ indicator-based measurements of seawater pH. Mar. Chem. 109:18-28 [doi:10.1016/j.marchem.2007.11.013].

Shitashima, K., M. Kyo, Y. Koike, and H. Henmi. 2002. Development of in situ pH sensor using ISFET, p. 106-108. *In* Proceedings of the 2002 International Symposium on Underwater Technology; 2002 Apr 16–19; Tokyo. IEEE.

―――, Y. Maeda, Y. Koike, and T. Ohsumi. 2008. Natural analogue of the rise and dissolution of liquid CO_2 in the ocean. Int. J. Greenhouse Gas Control 2:95-104 [doi:10.1016/S1750-5836(07)00092-8].

Wang, M., and S. Yao. 2003. Carbonate-melt oxidized iridium wire for pH sensing. Electroanalysis 15:1606-1615 [doi:10.1002/elan.200302723].

Zhu, Q., R. C. Aller, and Y. Fan. 2005. High-performance planar pH fluorosensor for two-dimensional pH measurements in marine sediment and water. Environ. Sci. Technol. 39:8906-8911 [doi:10.1021/es051023m].